5 Rare Kaon Decays at Brookhaven AGS

H. Kaspar (visiting scientist), P. Robmann, A. van der Schaaf,
S. Scheu, A. Sher and P. Truöl

The two projects discussed below exploit the unique low-momentum neutral and charged kaon beams available at Brookhaven National Laboratory's Allernating Gradient Synchrotron (AGS). Although BNL E-865 finished data-taking four years ago the analysis of the huge amount of recorded data is still in progress. KOPIO on the other hand is still in its planning phase. The experiment has been approved both by BNL and the U.S. National Science Foundation which reserved major funds for the combined MECO/KOPIO proposal [21]. MECO is a new search for $\mu - e$ conversion down to a sensitivity level of 10^{-16}.

5.1 BNL E-865: a search for lepton flavor violation in K^+ decay.

in collaboration with:
Paul–Scherrer–Institut, CH-5234 Villigen, Brookhaven National Laboratory, Upton, NY-11973, USA, University of New Mexico, Albuquerque, NM-87131, USA, University of Pittsburgh, Pittsburgh, PA-15260, USA, Yale University, New Haven, CT-06511, USA, Institute for Nuclear Research, Academy of Sciences 117 312 Moscow, Russia

While the analysis of the data for the lepton flavor violating decay $K^+ \to \pi^+\mu^+e^-$ ($K_{\pi\mu e}$), the primary goal of experiment E-865 at the Brookhaven AGS [1], is still in progress, the analysis of two further decay channels recorded in parallel has been concluded last year.

5.1.1 $K^+ \to \pi^+\pi^-e^+\nu_e$

The analysis of the $K^+ \to \pi^+\pi^-e^+\nu_e$ (K_{e4}) event sample has been published [2]. As reported already last year we collected more than ten times the number of events for this decay channel than all previous experiments combined. The model independent analysis of these data yielded the momentum dependence of the form factors of the hadronic currents as well as $\pi\pi$ scattering phase shifts. The form factors and phase shifts have served as an important input in the program to determine the couplings of the effective Hamiltonian of chiral QCD perturbation theory (ChPT) at low energies [3]. Furthermore, tight bounds on the value of the quark condensate, the fundamental order parameter of ChPT have been extracted [4]. Based on a suggestion of the authors of Ref. [4] we have slightly extended our analysis for our publication. The phase shifts can be related to the s-wave scattering lengths a_0^0 and a_0^2 for the isospin $I = 0$ and the $I = 2$ channel, respectively, using analyticity via the so-called Roy equations [5]. The values of the scattering lengths are restricted to a band in the a_0^0 versus a_0^2 plane by analyticity[5]:

$$a_0^2 = -0.0849 + 0.232a_0^0 - 0.0865(a_0^0)^2 \quad [\pm 0.0088] \ .$$

The centroid of this band is known in the literature as the *universal curve* [6]. The allowed region reduces considerably, if chiral symmetry constraints are imposed [4]:

$$a_0^2 = -0.0444 + 0.236(a_0^0 - 0.22) - 0.061(a_0^0 - 0.22)^2 - 9.9(a_0^0 - 0.22)^3 \quad [\pm 0.0008] \ .$$

From analyticity alone we obtain the result quoted last year:

$$a_0^0 = 0.228 \pm 0.012(\text{stat.}) \pm 0.003(\text{syst.})^{+0.006}_{-0.012}(\text{theor.}) \ , \tag{5.1}$$

while with the chiral symmetry constraints, we obtain:

$$a_0^0 = 0.216 \pm 0.013(\text{stat.}) \pm 0.004(\text{syst.}) \pm 0.005(\text{theor.}) \; . \tag{5.2}$$

This value agrees well with the latest ChPT prediction ($a_0^0 = 0.220 \pm 0.005$ [7]).

5.1.2 $K^+ \to \mu^+\nu_\mu e^+e^-$ and $K^+ \to e^+\nu_e e^+e^-$

Radiative kaon decays similar to radiative pion decays, which we investigated at PSI in the past [8, 9], play a special rôle in the ChPT program, because they serve both as an important test and as a source of input parameters for the theory. Compared to the decay modes with real photons $K^+ \to e^+\nu_e\gamma$ ($K_{e2\gamma}$) and $K^+ \to \mu^+\nu_\mu\gamma$ ($K_{\mu 2\gamma}$) the decays accompanied by a virtual photon turning into an electron-positron pair $K^+ \to \ell^+\nu_\ell e^+e^-$ (K_{e2ee}, $K_{\mu 2ee}$) allow a more detailed investigation into the structure of these decays. Our data [10] constitute a 100- and 150-fold increase in the number of events over previously published samples [11] for K_{e2ee} and $K_{\mu 2ee}$, respectively.

K_{e2ee} and $K_{\mu 2ee}$ decays are assumed to proceed via exchange of a W^+-boson ($\to \ell^+\nu$) and a photon ($\to e^+e^-$). The decay amplitude[12, 13] includes inner bremsstrahlung (IB), corresponding to the diagrams in Fig.5.1a,b and structure dependent (SD) radiation (Fig.5.1c), parameterised by vector F_V, axial-vector F_A, and R form factors. $K_{e2\gamma}$ and $K_{\mu 2\gamma}$ experiments [14] were only sensitive to $|F_V + F_A|$. R has not yet been measured, because it contributes only to decays with an e^+e^--pair. It can, however, be related to the kaon decay constant, $F_K = 160$ MeV, and the charge radius of the kaon $\langle r_K^2\rangle$[12]:

$$R = \frac{1}{3} M_K F_K \langle r_K^2\rangle \; .$$

The IB contribution is unambiguously determined by F_K. Since this contribution is helicity

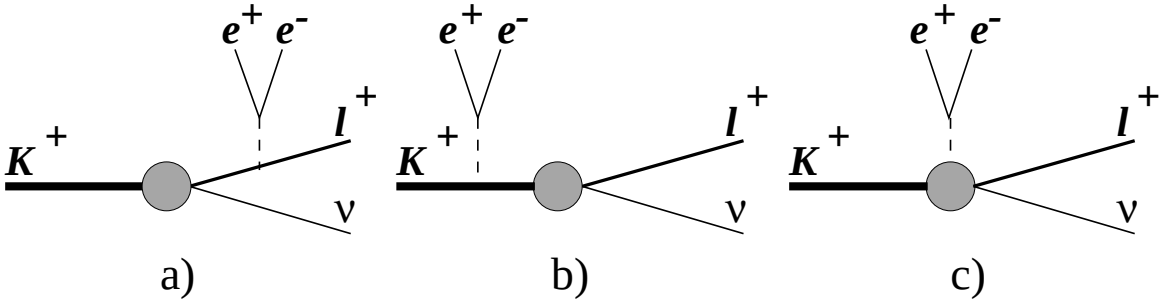

Figure 5.1: *$K^+ \to \ell\nu_\ell e^+e^-$ decay diagrams: a) and b) describe contributions from inner Bremsstrahlung, c) represents the structure dependent contribution.*

suppressed it is negligible in the K_{e2ee} decay whereas it contributes to about 60% of the $K_{\mu 2ee}$ branching ratio for invariant masses $m_{ee} > 145$ MeV. An additional 20% comes from the interference between IB and SD amplitudes. This interference makes it possible to determine the signs of all form factors relative to F_K.

The K_{e2ee} and $K_{\mu 2ee}$ data were obtained in the 1996 run together with the $K^+ \to \pi^+e^+e^-$ ($K_{\pi ee}$) data [15]. The trigger pre-selected events with three charged tracks, including an e^+e^- pair with high invariant mass m_{ee}. Off-line the K_{e2ee} and $K_{\mu 2ee}$ events were selected as those with small missing neutrino mass, m_ν, calculated from the momenta of the identified decay products and the nominal beam momentum, known from $K^+ \to \pi^+\pi^-\pi^+$ decays with an

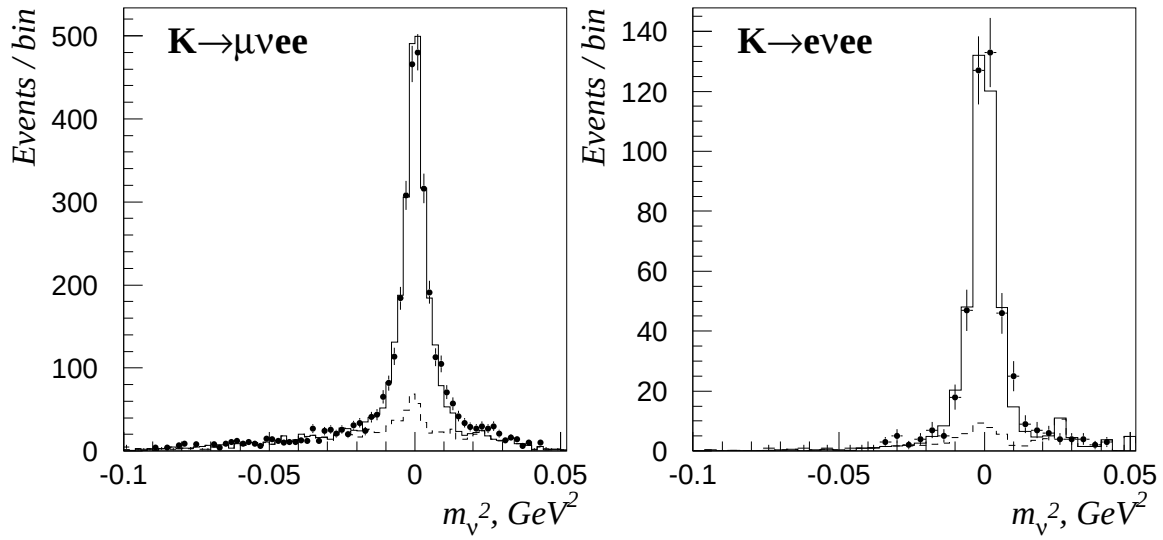

Figure 5.2: *Missing mass distributions for $K_{\mu 2ee}$ and K_{e2ee} decays. Points with error bars correspond to measured data, dashed lines indicate background, and solid lines represent the simulated distributions.*

uncertainty $\sigma_p/p = 1.3\%$ and $\sigma_{\theta x} = \sigma_{\theta y} = 4$ mrad. The m_ν^2 distribution is displayed in Fig.5.2. A cut $|m_\nu^2| < 0.016$ GeV^2 was used to isolate $K_{\ell 2ee}$ decays.

Background in both cases was dominated by accidental tracks accompanying a decay. By selecting events out of time for one of the tracks, we were able to obtain model independent samples of this background. The samples were normalised in the region $m_\nu^2 < -0.03$ GeV^2. The accuracies of normalisation, 8% for $K_{\mu 2ee}$ and 25% for K_{e2ee}, were sufficient for this purpose. To eliminate backgrounds associated with large branching ratio processes, *e.g.* $K \to \pi\pi_D^0$, cuts on the invariant e^+e^- mass > 145 MeV ($K_{\mu 2ee}$) and > 150 MeV (K_{e2ee}) were applied. The remaining background levels were determined from Monte Carlo simulation. The normalisation sample stems from pre-scaled K^+-decays with a π^0 in the final state followed by Dalitz decay $\pi_D^0 \to e^+e^-\gamma$ with a low invariant mass m_{ee}. Table 5.1 summarises the events samples. Using the calculated relative efficiencies for signal and normalisation

Table 5.1: *$K_{\ell\nu_\ell e^+e^-}$ event samples for signal and normalisation.*

Data sample	K_{e2ee}	$K_{\mu 2ee}$
Total	410	2679
Accidentals	35	355
$\pi^+e^+e^-$	5	126
$\pi^+\pi_D^0\pi_D^0$		33
Signal	370	2169

Normalisation sample	K_{e2ee}	$K_{\mu 2ee}$
$e^+\nu_e\pi_D^0$	86000	
$\mu^+\nu_e\pi_D^0$		16200
$\pi^+\pi_D^0$	2300	800
$\pi^+\pi^0\pi_D^0$		3000
Accidentals		400

channels and the number of events in Table 5.1 the following branching ratios were obtained:

$$K_{e2ee}: \quad (2.48 \pm 0.14\ (\text{stat.}) \pm 0.14\ (\text{syst.})) \times 10^{-8} \ \ (m_{ee} > 150\ \text{MeV}) \ ,$$

$$K_{\mu 2ee}; \quad (7.06 \pm 0.16 \pm\ (\text{stat.})0.26\ (\text{syst.})) \times 10^{-8} \ \ (m_{ee} > 145\ \text{MeV}) \ .$$

The event distributions were used to fit the three form factors F_A, F_V and R, assuming that all three depend in the same way on W^2, the effective mass of the $\ell^+\nu_\ell$-pair, and q^2, the

effective mass of the photon (e^+e^- pair). For the small mass ranges which are relevant here it suffices to consider only the low lying resonances [12]:

$$F_{V,A,R}^{(q^2,W^2)} = F_{V,A,R} \,/\, [(1 - q^2/m_\rho^2)(1 - W^2/\tilde{m}^2)] \,,$$

where $m_\rho = 770$ MeV, and $\tilde{m} = m_{K^*} = 892$ MeV for F_V and $\tilde{m} = m_{K_1} = 1270$ MeV for F_A, R. For further details we refer to Ref. [10]. Table 5.2 lists our results, which are in good agreement with both theoretical expectations and previous experimental results, where available.

F_V is related to the so-called axial anomaly: $F_V = \sqrt{2}M_K/8\pi^2F$ [12], while R can be obtained from the measured kaon charge radius $\langle r_K^2 \rangle = 0.34 \pm 0.05$ fm^2 [16]. If we use our value of R we obtain $\langle r_K^2 \rangle = 0.333 \pm 0.027$ fm^2. The difference with respect to the pion charge radius $\langle r_\pi^2 \rangle = 0.439 \pm 0.008$ fm^2 [17] disagrees with the ChPT $\mathcal{O}(p^4)$ relationship

Table 5.2: *Results for the form factors F_V, F_A, and R (in units of 10^{-3}; errors are $\pm$stat. $\pm$ syst. $\pm$ model). For comparison to previous experiments and because there exists a correlation between the form factor results the linear combinations $F_V \pm F_A$ are also listed.*

	$K^+ \to \mu^+\nu e^+e^-$	$K^+ \to e^+\nu e^+e^-$	Combined Fit	Expected	
F_V	$124 \pm 19 \pm 13 \pm 4$	$87 \pm 30 \pm 8 \pm 5$	$112 \pm 15 \pm 10 \pm 3$	96	[a]
F_A	$31 \pm 21 \pm 14 \pm 5$	$38 \pm 29 \pm 11 \pm 3$	$35 \pm 14 \pm 13 \pm 3$	48 ± 6	[b]
R	$235 \pm 25 \pm 14 \pm 12$	$227 \pm 20 \pm 10 \pm 8$	$227 \pm 13 \pm 10 \pm 9$	230 ± 34	[c]
$F_V + F_A$	$155 \pm 25 \pm 21 \pm 5$	$125 \pm 38 \pm 12 \pm 3$	$147 \pm 21 \pm 15 \pm 4$	144 ± 9	[14]
$F_V - F_A$	$93 \pm 32 \pm 17 \pm 7$	$50 \pm 44 \pm 15 \pm 7$	$77 \pm 20 \pm 19 \pm 6$	102 ± 74	[14]

[a] Theoretical value from the axial anomaly, see text;

[b] deduced from $\gamma = F_A/F_V = 0.522 \pm 0.050$ measured in a $\pi \to e\nu\gamma$ experiment [8];

[c] calculated from the measured $\langle r_K^2 \rangle$, see text.

$\langle r_\pi^2 \rangle - \langle r_K^2 \rangle = (1/32\pi^2F^2) \ln (M_K^2/m_\pi^2) = 0.036$ fm^2 [13].

5.1.3 $K^+ \to \pi^+\mu^\pm e^\mp$

The analysis of the final $K_{\pi\mu e}$ run dating from 1998, which is the thesis project of Aleksey Sher, is nearing completion. We expect to improve the sensitivity by at least a factor of three beyond our published limit of 2.8×10^{-11} [18]. Potential accidental background is studied using $K^+ \to \pi^+\pi^-\pi^+$ and $K^+ \to \pi_D^0 X$ calibration data. Background may be caused by combining a charged particle pair from one decay with a third track from another decay. To minimize these, the timing calibrations have been redone combining smaller groups of runs. This leads to an adjustment of the likelihood functions entering the final analysis.

The *blind* analysis philosophy is followed here, i.e. possible signal candidates are only looked for at the very end, after all tools have been established independently. We expect to *open the box* in summer 2002.

5.2 KOPIO: a study of the CP-violating rare decay $K_l^0 \to \pi^0\nu\overline{\nu}$

in collaboration with:
Brookhaven National Laboratory, University of Cincinatti, INR Moscow, KEK, Kyoto University of Education, Kyoto University, University of New Mexico, INFN University of Perugia, Stony Brook University, Thomas Jefferson National Accelerator Facility, TRIUMF/UBC, University of Virginia, Virginia Polytechnic Institute & State University, and Yale University.

5.2.1 CP-violation in the neutral K system

Since the early sixties it is known that the observed neutral kaon states are asymmetric mixtures of the strangeness eigenstates $K^0 = (d, \overline{s})$ and $\overline{K^0} = (\overline{d}, s)$:

$$\begin{aligned} K_s &= \tfrac{1}{\sqrt{2(1+\epsilon^2)}}((1+\epsilon)|K^0> + (1-\epsilon)|\overline{K^0}>) \\ K_l &= \tfrac{1}{\sqrt{2(1+\epsilon^2)}}((1+\epsilon)|K^0> - (1-\epsilon)|\overline{K^0}>) \end{aligned}$$

This so-called *indirect CP-violation* results from the difference in amplitudes for $K^0 \to \overline{K^0}$ and $\overline{K^0} \to K^0$:

$$\epsilon = \frac{<\overline{K^0}|H_{eff}|K^0> - <K^0|H_{eff}|\overline{K^0}>}{2(m_l - m_s) - i(\Gamma_l - \Gamma_s)}$$

Experimentally ($\epsilon = |\epsilon|e^{i\varphi_\epsilon}$):

$$|\epsilon| = (2.25 \pm 0.08) \times 10^{-3} \ , \quad \varphi_\epsilon = (43.5 \pm 0.1)^o \ .$$

An additional source of CP-violation, *direct CP-violation*, is found in a dependence of the amount of CP-violation on a specific final state, i.e. a difference between η_{+-} and η_{00} defined as:

$$\eta_{+-} \equiv \frac{<\pi^+\pi^-|H_{eff}|K_l>}{<\pi^+\pi^-|H_{eff}|K_s>} = \epsilon + \epsilon' \quad \eta_{00} \equiv \frac{<\pi^0\pi^0|H_{eff}|K_l>}{<\pi^0\pi^0|H_{eff}|K_s>} = \epsilon - 2\epsilon'$$

Only recently, after a long series of attempts an unambiguous signal for ϵ' was found [19, 20]. Unfortunately, the theoretical uncertainties in the standard model prediction are so large that the result can not yet be used as a constraint on physics beyond the standard model.

Within the standard model flavor mixing in W exchange is described by the complex 3×3 CKM matrix. Although the model makes no predictions for the values of the various elements the number of free parameters is reduced to four by constraints from unitarity, i.e. three angles and a phase. This is examplified by a very popular parametrization of the CKM matrix which is due to Lincoln Wolfenstein:

$$\begin{pmatrix} V_{ud} & V_{us} & V_{ub} \\ V_{cd} & V_{cs} & V_{cb} \\ V_{td} & V_{ts} & V_{tb} \end{pmatrix} = \begin{pmatrix} 1-\lambda^2/2 & \lambda & A\lambda^3(\rho - i\eta) \\ -\lambda & 1-\lambda^2/2 & A\lambda^2 \\ A\lambda^3(1-\rho-i\eta) & -A\lambda^2 & 1 \end{pmatrix}$$

Empirically $A = O(1)$, $\lambda, \rho, \eta = O(0.1)$. All CP-violating observables are proportional to $A^2\lambda^6\eta$. Constraints on the values of ρ and η are generally correlated, i.e. can be described by hyperbolic and circular regions in the ρ, η plane. Since the standard model makes no predictions for the CKM matrix all that can be done at present is check the consistency of the description, i.e. see whether the various observables can be described by a single set of values. It is very fortunate that we may expect significant improvements in the experimental constraints, both from the K and the B sector, in the next decade so that meaningful tests

can be made.

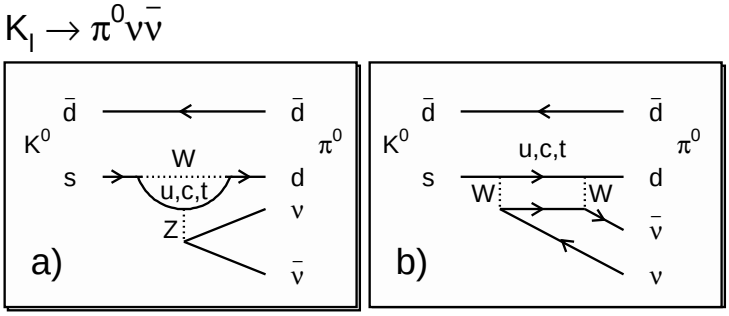

Figure 5.3: *Leading diagrams inducing* $K_l^0 \to \pi^0\nu\overline{\nu}$.

The decay $K_l \to \pi^0\nu\overline{\nu}$ plays a special role in this program. As is illustrated in Fig.5.3 the process has major contributions from penguin and box diagrams with up-type quarks in the intermediate state. Since the transition amplitude scales with the quark mass the top contribution dominates by far and:

$$A(K_l \to \pi^0\nu\overline{\nu}) \propto V_{td}^* V_{ts} - V_{ts}^* V_{td} \propto i\eta \ ,$$

so:

$$B(K_l \to \pi^0\nu\overline{\nu}) \propto \eta^2.$$

The branching ratio is thus a direct measure of η^2 without "background" from CP conservation or indirect CP violation. The price to pay is a very low branching ratio ($\approx 3 \times 10^{-11}$) and a very weak all-neutral event signature. Experimentally only an upper limit was found until now [22], more than four orders of magnitude above the expectation.

The corresponding charged decay mode does not require CP violation but gives a circular constraint around $\rho = 1.3, \eta = 0$:

$$B(K^+ \to \pi^+\nu\overline{\nu}) \propto (\rho - 1.3)^2 + \eta^2.$$

Until recently BNL E-787 found two event candidates [23].

5.2.2 Overview of the KOPIO experiment

Two photons with the invariant mass of a π_0 and nothing else is the signature for a $K_{\pi\nu\nu}$ decay. The KOPIO proposal [21] explains in detail, how this signature is used to isolate this ultrarare decay mode from the background. Here we summarize the basic features.

The most important aspect of the experiment is the use of a low momentum short-pulse K_L^0 beam, whose momentum can be determined event by event via time-of-flight. The observed π^0, reconstructed from the energy, direction and common vertex of the two photons from its decay, can then be transformed into the K_L^0 center-of-mass system, and kinematic constraints can be applied, allowing to distinguish the events of interest from the dominant background source $K_L^0 \to \pi^0\pi^0$. Figure 5.4 shows a sketch of the planned detector.

A 24 GeV primary proton beam from the AGS strikes the production target in 200 ps wide pulses separated by 40 ns. Neutral particles emerging from the target at angles around 48° in the horizontal plane may reach the experiment starting 9 m downstream. Under these conditions the K_L^0 momentum spectrum at the decay region peaks at 650 MeV/c. Vertically the beam is collimated into a narrow band, to limit the beam halo and to provide another vertex reconstruction constraint. 16% of the kaons decay within the 4 m long evacuated decay region, which is surrounded by the π^0 detector and the various charged-particle and photon veto systems. The π^0 detector consists of a highly segmented preradiator followed by an electromagnetic calorimeter. The arrival time, position and angle of each photon is

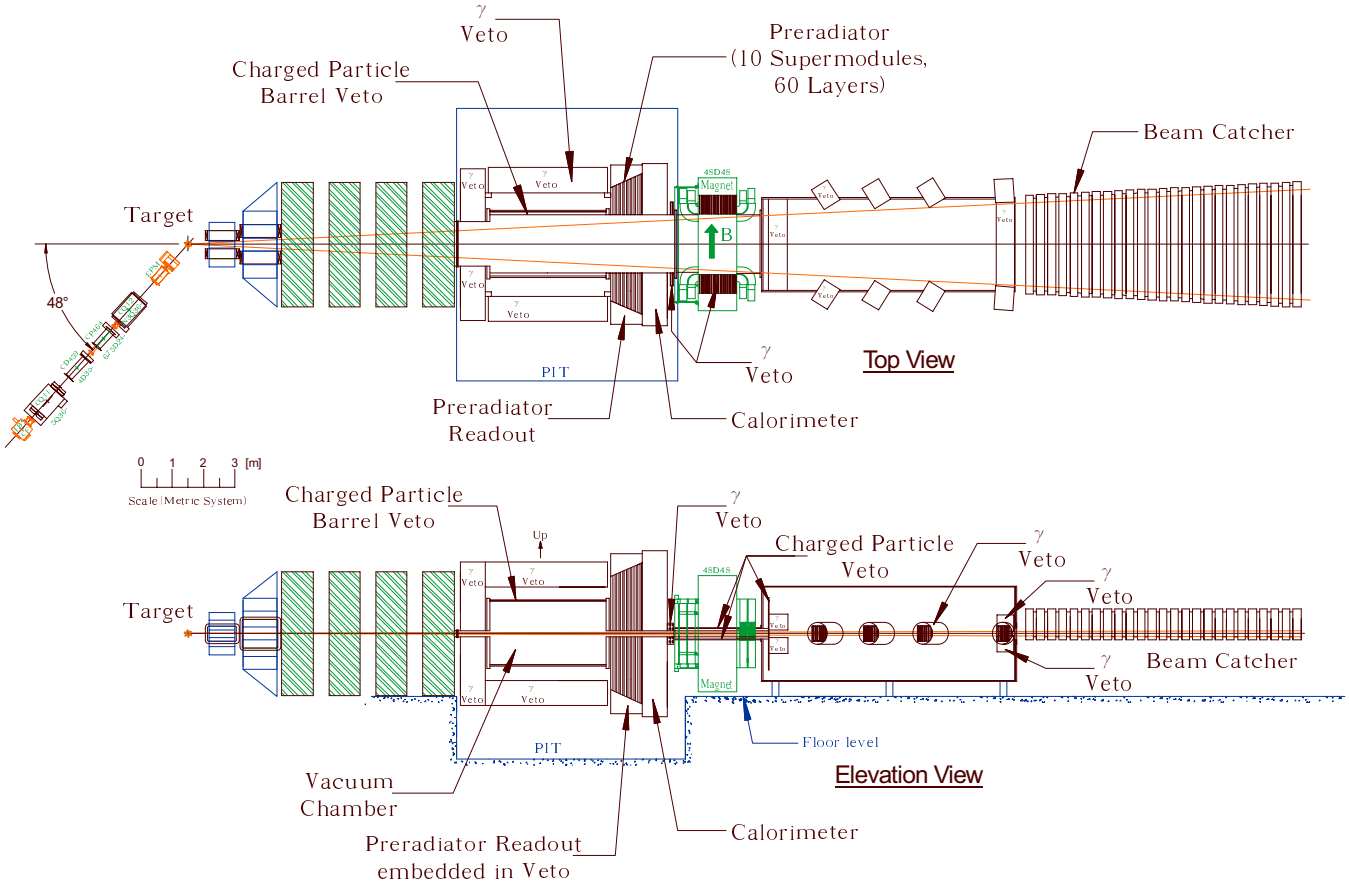

Figure 5.4: *Plan and elevation views of the KOPIO detector.*

determined in the preradiator by recontruction of the trajectories of the initial e^+e^- pairs. The photon energies are determined by combining the signals observed in the preradiator with those from the calorimeter. A resolution of $\sigma_E/E \approx 0.033/\sqrt{E}$ is expected.

The Zurich group took over the responsibility for the charged-particle veto system situated directly around the decay region. In the following we discuss the requirements to this system and some other considerations that should lead to a specific design.

5.2.3 The KOPIO charged particle veto system

The purpose of the charge-particle veto system is the efficient identification of background processes in which an apparent $\pi^0 \to 2\gamma$ decay inside the decay volume is accompanied by charged particle emission. Examples of such background processes are, (i) $K_L \to \pi^+\pi^-\pi^0$, (ii) $K_L \to e^+\pi^-\nu\gamma$ in which the positron creates a second photon through Bremsstrahlung or annihilation in flight, (iii) $K_L \to e^+\pi^-\nu$ again followed by $e^+ \to \gamma$ whereas the π^- creates a photon through $\pi^- p \to \pi^0 n$. In all cases two particles with opposite electrical charge emerge. In all cases the events may also produce signals in other detector elements, like the barrel veto system. Detection efficiencies of 99.99% or better are required to keep these backgrounds below a few events in the final sample.

The charged-particle veto system will consist of two or three layers of plastic scintillator mounted inside the vacuum tank surrounding the decay volume. The detectors will be separated from the high-quality beam vacuum by a thin metallic foil.

5.2.4 Response of plastic scintillator to $\pi^\pm$ at 185 - 360 MeV/c

In spring 2001 we measured the response of plastic scintillator to $\pi^\pm$, $\mu^\pm$ and $e^\pm$ at momenta between 185 and 360 MeV/c. The purpose of these studies performed at PSI was twofold, (i) determination of the fundamental limitations to the detection efficiency associated with processes (such as pion absorption or positron annihilation in flight) that result in a partial or complete loss of scintillator signal, and (ii) tests of detector prototypes, in particular of scintillators with embedded wave-length-shifting fibres. For a detailed discussion see Ref.[24].

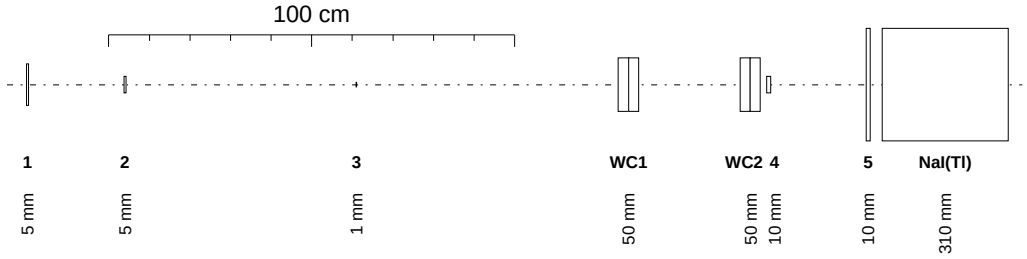

Figure 5.5: *Setup for the study of the response of plastic scintillator to $\pi^\pm$, $\mu^\pm$ and $e^\pm$. 1-5: plastic scintillators; WC1/2: x-y proportional wire chambers (1mm spacing). The values on the bottom denote the thickness of the corresponding detector. The beam enters from the left.*

Figure 5.5 shows the experimental setup which consists of a particle defining telescope (counters 1-3 and $x-y$ multiwire proportional chambers WC1 and WC2) followed by a veto system consisting of two plastic scintillation detectors (4 and 5) and a NaI(Tl) crystal.

Particle identification was done on the basis of time of flight between the production target and detector 2. The resulting samples have purities of 99.9% or better. Events were selected with trajectories pointing both at counter 3 and counter 4. Figure 5.6 shows the corresponding NaI(Tl) energy distributions for $e^\pm$ and $\pi^\pm$. The muon spectra are very similar to those observed for $e^\pm$. Whereas 99% of the electrons and positrons produce signals in

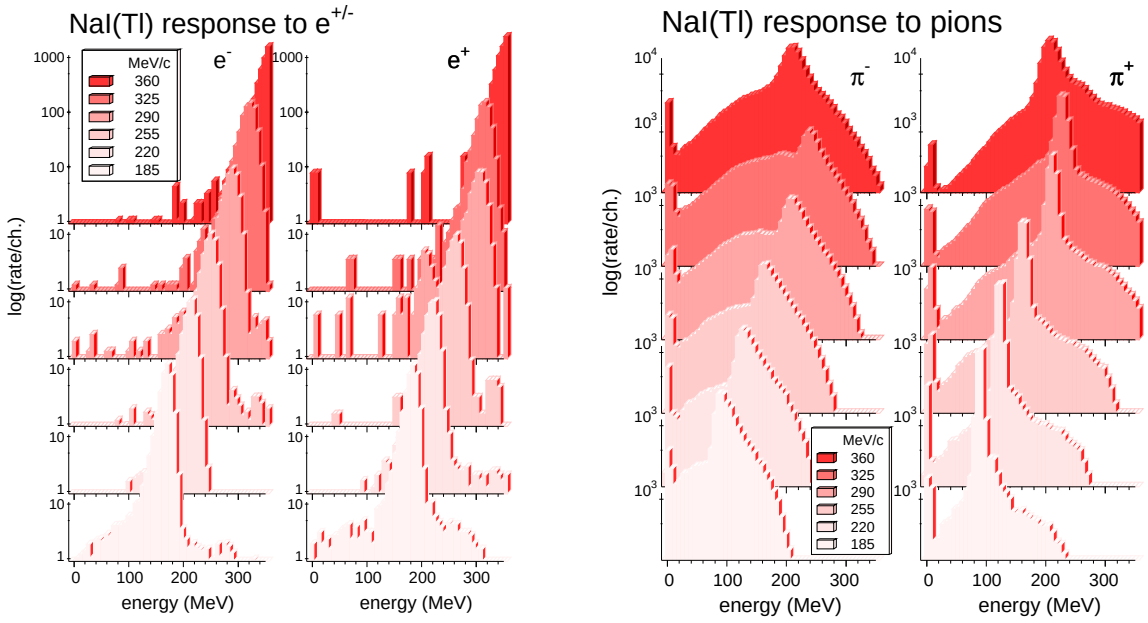

Figure 5.6: *NaI(Tl) response to $e^\pm$ and $\pi^\pm$ at momenta in the range 185-360 MeV/c. At 360 MeV/c pions may cross the detector resulting in a reduction in energy deposit.*

the full-energy peak with no indication of a pedestal peak, pions may disappear by nuclear

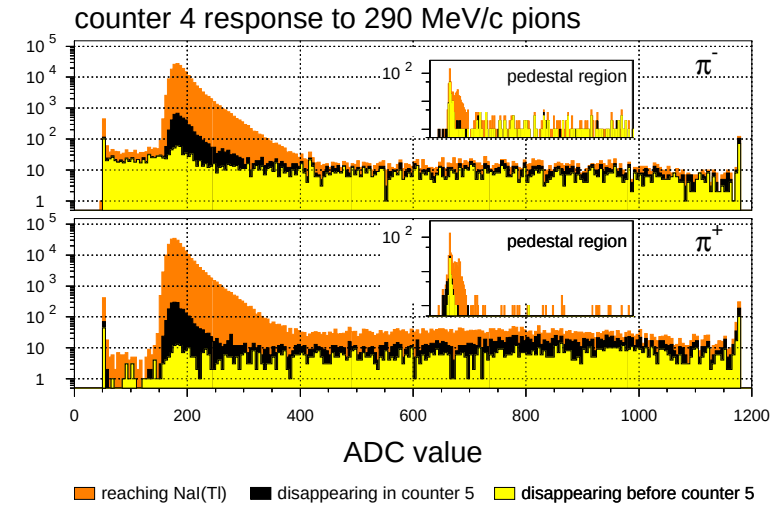

Figure 5.7: *Response of counter 4 to 290 MeV/c $\pi^{\pm}$ for, (i) all events with trajectories pointing at counter 4, (ii) the subset of (i) contained in the NaI(Tl) pedestal peak (see Fig. 5.6), and (iii) the subset of (ii) contained in the pedestal peak of counter 5.*

reactions resulting in a broad continuum. In 1-3% of the cases no signal is seen at all. These events are caused by interactions in counters 4 and 5 (total thickness 15 mm).

Figure 5.7 shows various distributions of the signals produced by 290 MeV/c pions in counter 4. Similar spectra are observed at the other momenta. Events without signals in counter 5 and NaI(Tl) are characterised by flat distributions with a small peak contribution caused by interactions in the dead layer between counters 4 and 5. Note the striking difference between π^+ and π^- in the event rate at the low side of the peak: whereas π^- interactions often lead to neutral final states π^+ is known to produce one or more low-energy protons which result in additional scintillation light. From the observation that the pedestal peak has similar strengths for both polarities one must conclude that these secondary charged particles tend to have relatively short ranges.

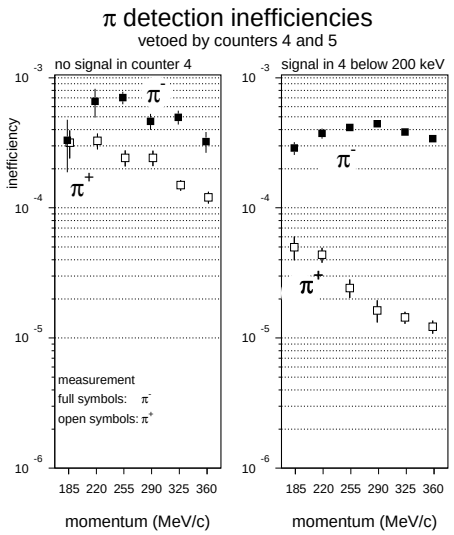

Figure 5.8: *Pion detection inefficiency caused by interactions in WC2 and the wrapping of counter 4 and by a 200 keV detection threshold on the signal in counter 4. Results are shown for the case that counter 5 is used as veto counter too. When also NaI(Tl) is used as veto counter the inefficiencies drop by up to 50%.*

The observed pion detection inefficiencies are plotted against beam momentum in Fig. 5.8. We conclude that detection inefficiencies of $O(10^{-4})$ for momenta around 300 MeV/c could be obtained if (i), the dead layer in front of the veto system (which includes the window separating the detector from the high-vacuum decay region) could be kept below 20 mg/cm^2 and (ii), a detection threshold of ≈ 75 keV (corresponding to ≈ 0.3 mm scintillator thickness) could be reached. Meeting this performance seems neither trivial nor hopeless. Most critical parameter is the yield of photo-electrons per energy deposit (see Sec. 5.2.5). The detection efficiencies for $e^{\pm}$ and $\mu^{\pm}$ would always be better than for pions. At most momenta we found lower limits only.

5.2.5 Experience with a first detector prototype

At present we plan to equip the charged particle barrel veto with 2-3 detector layers for which two options are considered:

- Scintillator bars with dimensions typically $400 \times 50 \times 5$ mm^3. These detector elements would be coupled through short light guides to miniature photomultipliers mounted inside the vacuum tank. Active elements inside the vacuum tank increase the time required in case of repair. Also care has to be taken to avoid break-through of the photomultiplier high voltage. At the other hand the detector threshold which is the main figure of merit might be significantly lower than for option 2.

- Scintillator tiles with dimensions typically $400 \times 100 \times 5$ mm^3. The scintillation light would be extracted with the help of wave-length-shifting fibres glued in grooves of 1 mm depth and 5-10 mm spacing. The fibres would be coupled to multi-channel hybrid photomultipliers mounted on the outside of the vacuum tank. We have tested this option both in the beam and with cosmic rays. The observed number of photo-electrons ($\approx$ 100 in 10 mm scintillator) is compared with predictions in Fig.5.9.

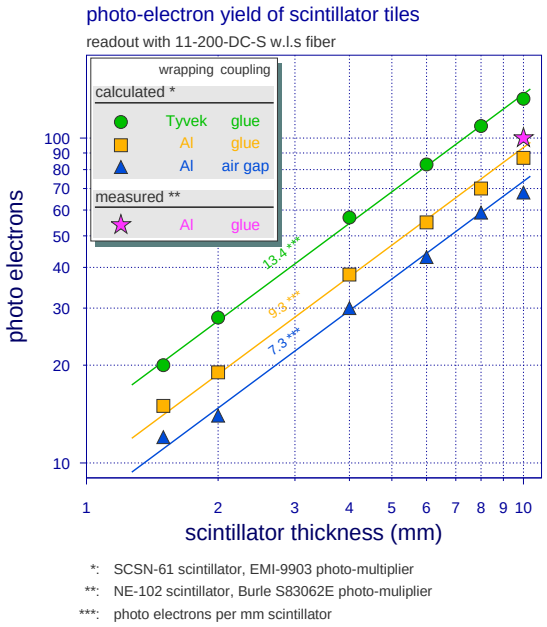

Figure 5.9: *Mean number of photo-electrons for minimum-ionising particles crossing a scintillator tile with embedded wave-length-shifting fibres. Our measured value is compared with predictions for similar configurations by [25].*

The value of $\approx$ 100 photo-electrons for minimum ionising particles crossing 10 mm of scintillator read out with embedded w.l.s. fibre corresponds to 3 photo-electrons for a 75 keV threshold. The sensitivity of counter 4 which was viewed through a classical fishtail light guide is about 20 times higher and for this reason we intend to make a critical comparison between full-scale prototypes of both types of detector.

References

[1] *A Large Acceptance, High Resolution Detector for Rare K^+-decay Experiments*, R. Appel *et al.*, Nucl. Instr. Meth. **A479** (2002), 340.

[2] *A New Measurement of K^+_{e4} Decay and the $s-$Wave $\pi\pi$ Scattering Length*, S. Pislak *et al.*, Phys. Rev. Lett. **87** (2001), 221801.

[3] G. Amoros, J. Bijnens, and P. Talavera, Phys. Lett. **B480**,71 (2000); Nucl. Phys. **B595**, 293 (2000); err. **B598**, 665 (2001); ibid. **B602**, 87 (2001).

[4] G. Colangelo, J. Gasser, and H. Leutwyler, Phys. Rev Lett. **86**, 5008 (2001).

[5] B. Ananthanarayan *et al.*, Phys. Rep. **353/4**, 207 (2001).

[6] D. Morgan, and G. Shaw, Nucl. Phys. **B10**, 261 (1969).

[7] G. Colangelo, J. Gasser, and H. Leutwyler, Phys. Lett.**B488**, 261 (2000).

[8] A. Bay *et al.*, Phys. Lett. **B174** (1986), 445.

[9] S. Egli *et al.*, Phys. Lett. **B222** (1989), 533.

[10] *Experimental Study of the Radiative Decays* $K^+ \to \mu^+\nu_\mu e^+e^-$ *and* $K^+ \to e^+\nu_e e^+e^-$, A.A. Poblaguev *et al.*, hep-ex 0204006, submitted to Phys. Rev. Lett. (2002).

[11] A.M. Diamant-Berger *et al.*, Phys. Lett. **62** (1976), 485.

[12] D. Bardin, and E. Ivanov, Sov. J. Part. Nucl. **7** (1976), 485.

[13] J. Bijnens, G. Ecker, and J. Gasser, Nucl. Phys. **396** (1993), 81.

[14] S. Adler *et al.*, Phys. Rev. Lett. **85** (2000), 2256; S. Heintze *et al.*, Nucl. Phys. **149** (1979), 365; K. Heard *et al.*, Phys. Lett. **B55** (1975), 324.

[15] R. Appel *et al.*, Phys. Rev. Lett. **83** (1999), 4482.

[16] S. Amendiola *et al.*, Phys. Lett. **B178** (1986), 435.

[17] S. Amendiola *et al.*, Nucl. Phys. **B277** (1986), 168.

[18] R. Appel *et al.*, Phys. Rev. Lett. **85** (2000), 2450.

[19] A. Lai *et al.*, Eur. J. Phys. **C22** (2001), 231.

[20] A. Alavi-Harati *et al.*, Phys. Rev. Lett. **83** (1999), 22.

[21] *Rare Symmetry Violating Processes*
Joined MECO/KOPIO proposal (1999), `http://pubweb.bnl.gov/people/rsvp`.

[22] A. Alavi-Harati et al., Phys. Rev. **D61** (2000), 072006.

[23] S. Adler *et al.*, E787 Collaboration, Phys. Rev. Lett. **88** (2002), 041803.

[24] H. Kaspar, P. Robmann, A. v.d. Schaaf, S. Scheu, P. Truöl, J. Egger, and M. Blecher, *Measurements on the response of plastic scintillator to charged pions at 185 - 360 MeV/c*, KOPIO techn. note tn027 (2001).

[25] V. Issakov, private communication.